Investigating the preservation of orbital forcing in peritidal carbonates

DAVID B. KEMP[1*], SASKIA M. VAN MANEN[2], DAVID A. POLLITT[3], PETER M. BURGESS[4]

[1]*School of Geosciences, University of Aberdeen, Old Aberdeen, AB24 3UE, UK*

[2]*Environment, Earth and Ecosystems, The Open University, Walton Hall, Milton Keynes, MK7 6AA, UK*

[3]*Chevron Corporation, 1500 Louisiana St., Houston, TX 77002, USA*

[4]*Department of Earth Sciences, Royal Holloway, University of London, Egham, TW20 0EX, UK*

*e-mail: david.kemp@abdn.ac.uk

Keywords: Milankovitch; orbital forcing; spectral analysis; peritidal carbonates; eustasy; modelling

ABSTRACT

Metre-scale cycles in ancient peritidal carbonate facies have long been thought to represent the product of shallow water carbonate accumulation under orbitally controlled sea level oscillations. The theory remains somewhat controversial, however, and a contrasting view is that these cycles are the product of intrinsic, and perhaps random, processes. Owing to this debate, it is important to understand the conditions that do, or do not, favour the preservation of orbital forcing, and the precise stratigraphical expression of that forcing. In this work, a one-dimensional forward model of carbonate accumulation is used to test the ability of orbitally paced sea level changes to reconstruct cyclicities and cycle stacking patterns observed in greenhouse peritidal carbonate successions. Importantly, the modelling specifically tests insolation-based sea level curves that likely best reflect the pattern and amplitude of sea level change in the absence of large-scale glacioeustasy. We find that such sea level histories can generate precession and eccentricity water depth/facies cycles in our models, as well as eccentricity-modulated cycles in precession cycle thicknesses (bundles). Nevertheless, preservation of orbital forcing is highly sensitive to carbonate production rates and amplitudes of sea level change, and the conditions best suited to preserving orbital cycles in facies/water depth are different to those best suited to preserving eccentricity-scale bundling. In addition, it can be demonstrated that the preservation of orbital forcing is commonly associated with both stratigraphic incompleteness (missing cycles) and complex cycle thickness distributions (e.g. exponential), with corresponding implications for the use of peritidal carbonate successions to build accurate astronomical timescales.

INTRODUCTION

Orbitally forced climate change is thought to be a primary driver of high-frequency sea level oscillations during both greenhouse and icehouse intervals of Earth history. Evidence for such a control has been deduced in particular from quantitative analysis of metre-scale, exposure-bound facies repetitions and stacking patterns in shallow water carbonate successions, which can exhibit cyclicities matching known orbital frequencies (Goldhammer *et al*., 1987, 1990; Preto *et al*., 2001; Yang and Lehrmann, 2003; Cozzi *et al*., 2005; Gil *et al*., 2009). Unambiguous recognition of orbital forcing is important as it permits the prediction of features of stratigraphic importance, such as facies types and thicknesses, and hiatus durations and distributions. Moreover, orbital cycles recognised stratigraphically provide a temporal framework for high-resolution timescale development and correlations. A contrasting view is that the stratigraphic architecture and facies patterns of peritidal successions can more readily be attributed to intrinsic, perhaps random, processes without appealing to a dominant orbital control (Algeo and Wilkinson, 1988; Drummond and Wilkinson, 1993a; Wilkinson *et al*., 1998; Burgess *et al*., 2001). The implications of an unordered stratigraphic record are negligible predictability, chronologic control and correlation potential. Both orbital forcing and stochastic processes likely contribute in varying degrees to the development of shallow water carbonate successions, and hence it is important to understand the conditions that do, or do not, favour the preservation of orbital cycles in a given succession. Moreover, it is important to understand how orbital forcing is expressed stratigraphically if it is to have the utility outlined above.

Forward modelling offers an opportunity to test the efficacy of orbital insolation forcing of sea level as a driving mechanism of shallow water carbonate sedimentation, and for establishing the conditions best suited to preservation of this forcing. To date, such modelling has largely taken an inverse approach, whereby the parameters governing the generation of real stratigraphies are reconstructed, often invoking only generalised sea level curves (e.g. stacked sine waves). As recognised by Forkner *et al*. (2010), these are unlikely to be representative of the true complexities and amplitudes of insolation driven sea level changes. The way orbitally controlled insolation drives sea level oscillations, and how these oscillations are translated and preserved in the sedimentary record, is not fully understood. In the case of peritidal carbonate successions deposited under largely ice-free climates, there is little consensus on the precise mechanistic link between insolation and eustasy, with climate driven changes in continental water storage, upland glacier volumes and seawater thermal expansion/contraction all cited as possible eustatic drivers (Jacobs and Sahagian, 1995; Schulz and Schäfer-Neth, 1997; Coe, 2003; Immenhauser, 2005).

Recent work has sought to address these issues. In particular, Forkner *et al.* (2010) utilised insolation signals as sea level proxies in predictive modelling of peritidal carbonates in an effort to better understand problematic successions such as the Latemar limestone platform of northern Italy, where the observed orbital-like pattern of stratigraphic cyclicity is ostensibly at odds with radiometric dating that suggests a younger duration than that implied by the orbital chronology. Kemp (2011) highlighted how using an insolation-like sea level signal within a one dimensional model can explain the sometimes high amplitude of inferred ~100 ka eccentricity cycles in shallow water successions (e.g. Preto *et al.*, 2001; Yang and Lehrmann, 2003; Preto *et al.*, 2004; Cozzi *et al.*, 2005; Gil *et al.*, 2009), despite eccentricity having a negligible effect on insolation. It was further noted that the use of an insolation-like sea level curve could reconstruct the observed stacking of precession cycles into eccentricity modulated hierarchies, or bundles (Kemp, 2011). Together, these observations obviate the need for invoking potentially unrealistic sea level histories consisting of separate eccentricity and precession components to reconstruct ancient shallow water carbonate stratigraphies (e.g. Goldhammer *et al.* 1987, 1990).

In this contribution, these ideas are developed further by employing a one-dimensional stratigraphic forward model of carbonate accumulation in an effort to help evaluate key controls that govern the preservation of statistically recognisable orbital cycles in strata. In so doing, the veracity of orbital insolation forcing of eustasy as a primary driver of ancient peritidal carbonate stratigraphies is assessed. Patterns of cyclicity in shallow water carbonate successions have traditionally been investigated in two ways: 1) analysis of cyclicity in facies repetitions ostensibly linked to oscillating water depths (e.g. Preto et al., 2001), and 2) analysis of cyclicity in the thickness variations of metre-scale, typically exposure-bound facies packages (so-called 'bundling', e.g. Hinnov and Goldhammer, 1991). Both approaches are explored in this work. To avoid confusion, and following Pollitt *et al*. (2014), an exposure-bound package of strata is described as a high frequency sequence (HFS). The term cycle is reserved for a statistically verified oscillation (i.e. of near constant period) in either inferred water depth or the thicknesses of HFSs. We also examine the nature of HFS thickness distributions in the successions generated by our modelling.

FORWARD MODEL

Our model is a one-dimensional process-response stratigraphic forward model of carbonate production and accumulation based on the Dougal model described in detail in Burgess and Pollitt (2012) and Pollitt *et al*. (2014) (see also Pollitt, 2008). The model records the vertical position of a carbonate platform at a single point in space such that:

$$h_t = s_{\Delta t} + p_{(w,\Delta t)} - d_{\Delta t}$$

where *h* is the platform height in metres, *t* is time in millions of years (Myr), *s* is linear subsidence rate in m Myr^{-1}, *p* is total carbonate production rate in m Myr^{-1}, *w* is water depth in metres (which mediates production rate), *d* is subaerial erosion rate in m Myr^{-1}, and Δt is the model time step. Since production relates linearly to accumulation, the model considers only aggradational platform growth, and does not account for progradation or sediment transport. Compaction is not accounted for. The use of a one-dimensional model of accumulation is suitable for the purposes of this study because of primary interest is the aggradation of strata in a one-dimensional column such as would be studied at outcrop or downhole cyclostratigraphically through regular measurements of facies/facies proxies and/or cycle thicknesses (e.g. Preto *et al*., 2001; Preto *et al*. 2004; Zühlke *et al*., 2003; Cozzi *et al*., 2005; Bosence *et al*., 2009; Wu *et al*., 2013). A further key benefit of the model, implemented here in Matlab, is short run-time, allowing the rapid generation of many hundreds of synthetic stratigraphic successions.

Carbonate production

Total carbonate production in the model over a given time step is simulated as the sum of three water depth dependent carbonate factories: euphotic, aphotic and oligophotic (*sensu* Pomar, 2001a; Fig. 1). Euphotic production dominates in shallow (<40 m) water depths and refers to production by autotrophic and autoheterotrophic organisms that require significant light. Oligophotic producers inhabit deeper waters with reduced light conditions and cooler temperatures (Pomar, 2001b). Aphotic carbonate production occurs via heterotrophic biota that do not require light, and which may live in a variety of water depths. In the model, carbonate production via the euphotic (e) pathway is based on the formulation of Bosscher and Schlager (1992), and modelled as:

$$e_{(t)} = e_{(m)} \cdot tanh\left(k \cdot exp\left(d \cdot w_{(t)}\right)\right)$$

where *t* is time, *w* is water depth in metres, *m* is the maximum production rate in m Myr^{-1}, *d* is a decay constant, *k* is a rate constant. For the oligophotic (*o*) factory, production is modelled via:

$$o_{(t)} = o_m \cdot tanh\left(k \cdot exp\left(d_u \cdot \left(r - w_{(t)}\right)\right)\right) \quad if \ \ w_{(t)} < r$$

OR

$$o_{(t)} = o_m \cdot tanh\left(r \cdot exp\left(d_l \cdot \left(w_{(t)} - r\right)\right)\right) \quad if \ \ w_{(t)} > r$$

where *t* is time, *w* is water depth in metres, *m* is the maximum production rate in m Myr^{-1}, *k* is an offset to the exponential curve, *d* is a decay constant, and *r* is a depth constant. The upper and lower decay constants (d_u and d_l) reflect how the upper and lower parts of the exponential curve have different rates of exponential decay. For the aphotic (*a*) factory, production is modelled via:

$$a_{(t)} = a_m \cdot \frac{w_{(t)}}{d} \quad if \quad w_{(t)} < x$$

OR

$$a_{(t)} = a_m \cdot 1 - \left(\frac{d - w_{(t)}}{d - j}\right) \cdot 1 - f \quad if \quad w_{(t)} < j \ AND \ w_{(t)} > x$$

ELSE

$$a_{(t)} = a_m \cdot f$$

where t is time, w is water depth in metres, m is the maximum production rate in m Myr^{-1}, d is the maximum production depth in m, j is the plateau production depth in m, and f is the plateau production rate as a proportion of m. The logical OR and ELSE operators are triggered if the water depth is greater than the turnaround depth constant x, and/or the plateau production depth constant j.

Following Pollitt *et al*. (2014), rates of euphotic carbonate production likely exceed rates achievable by oligophotic and aphotic factories, and hence total carbonate production as a function of water depth follows most closely the euphotic production curve (Fig. 1). Maximum oligophotic and aphotic production rates were set at 20% and 5% of the maximum euphotic rate respectively (Pollitt *et al*., 2014). In the model scenarios employed here, designed to replicate greenhouse depositional environments with low eustatic amplitudes (<20 m, e.g. Miller *et al*., 2005), euphotic production dominates, contributing to a minimum of 80% of the total carbonate production rate at water depths up to 10 m (Fig. 1).

Subsidence, erosion and exposure

Subsidence is a key parameter that governs long-term preservation of strata. Assuming a tectonically stable carbonate platform environment, subsidence is modelled using a constant rate of 100 m Myr^{-1} (Burgess and Pollitt, 2012). A second control on long-term preservation is erosion, and subaerial erosion in all model runs is fixed at 10 m Myr^{-1}. This relatively low rate reflects a) the generally rapid lithification of carbonate strata, and b) the fact that carbonate erosion over the relatively short exposure durations implied by orbitally forced sea level changes proceeds through localised dissolution and secondary porosity creation with limited changes in elevation (Enos, 1991). In studies of metre-scale shallow water carbonate cyclicity, evidence for exposure such as palaeosols, karst development and supratidal/littoral facies associations is used to define the boundaries of individual HFSs deemed to result from eustatic oscillations (e.g. Goldhammer *et al*., 1987, 1990; Cozzi *et al*., 2005; Gil *et al*., 2009; Eberli, 2013). In such successions, however, the evidence for exposure can be equivocal. Notably, there is a temporal dependence on the development of unambiguous exposure features (Schlager, 2004; 2010). Schlager (2004) estimated that the time required to generate geological evidence of exposure was at least 1 ka. For modelling purposes therefore, a HFS is further defined as a preserved package of strata bounded by exposure intervals of 1 ka or more.

Lag time

It has long been held that to reconstruct the commonly observed shallowing upward motif of metre-scale exposure bound carbonate cycles, carbonate production and/or accumulation must be suppressed or limited after a platform is initially flooded following exposure (e.g. Schlager, 1981; Read *et al*., 1986; Enos, 1991). The inclusion of modeled lag depths or lag times that reflect this delayed accumulation in stratigraphic models has been a longstanding way of reproducing shallowing upward patterns in real cycles (Read *et al*., 1986; Goldhammer *et al*., 1987; Enos, 1991; Burgess and Pollitt, 2012). Tipper (1997) and subsequently Blanchon and Blakeway (2003) argued that lags in carbonate deposition largely reflect patchy colonisation of a newly submerged platform, not representative of the response of the platform as a whole. Because the modelling approach used here seeks to replicate the cyclostratigraphic workflow of analysing platform stratigraphies in a single dimension either at outcrop or in cores, this lagged response of carbonate production to sea level rise would be readily observed (Blanchon and Blakeway, 2003). To replicate this, lag times recorded during successive episodes of submergence are drawn from a set of random times. This approach is conceptually similar to that adopted by Blanchon and Blakeway (2003), and produces lag times with a probability distribution close to that generated by these authors, with a mode centred between 1 and 2 ka, skewed towards shorter durations but with a tail up to ~4 ka (Fig. 2).

An insolation-based sea level curve

As discussed in the introduction, the precise mechanisms by which orbitally forced insolation signals are translated into sea level changes are poorly understood. Depending on the eustatic driver invoked (e.g. ice volume changes, temperature changes, groundwater storage changes), it is reasonable to expect differing transfer functions that relate insolation and eustasy, which may be non-linear and complex. For so-called greenhouse intervals of Earth history, the expected limitation in the size of any high-latitude ice sheets places an important limit on the attainable magnitudes of eustatic change, and non-glacially driven changes may not have exceeded ~10 m amplitude (Wright, 1992; Schulz and Schäfer-Neth, 1997; Miller *et al*., 2005; Sømme *et al*., 2009). Similarly, insolation forced changes in thermal expansion and contraction of seawater and/or terrestrial water retention and release would likely yield symmetrical changes in sea level, as opposed to the strongly asymmetrical sea level cycles that result from differential rates of ice-sheet growth and decay (Pittet, 1994; Hillgärtner and Strasser, 2003).

Following Forkner *et al*. (2010), greenhouse sea level change is modelled here as a linear translation of low latitude orbital forcing, which is dominated by ~21 ka precession forcing (Fig. 3). Importantly, previous work has indicated that such a signal does not preclude asymmetry in the resultant stratigraphic cyclicity (Hillgärtner and Strasser, 2003; Kemp, 2011). A random 1 Myr interval of the Laskar *et al*. (2004) insolation solution of summer insolation at 20°N (where modern carbonate production thrives) between 89.94 and 90.94 Ma (Fig. 3a) was extracted. To convert to eustasy, this signal (in units of W m^{-2}) was normalised to zero mean and with variance user defined in metre units (Fig. 3b).

Long-term (>1 Myr) eustatic trends are a ubiquitous phenomenon in both greenhouse and icehouse intervals, with amplitudes that exceed the variance of orbitally forced cycles (Harrison, 2002; Miller *et al*., 2005; Schlager, 2010; Ruban, 2014). Harrison (2002) determined the behaviour of sea level change across timescales of days to millions of years, and found that sea level change is consistent with a random walk process with superimposed orbital cyclicity (Harrison, 2002; see also Schlager, 2010). These findings emphasise the likely importance of non-periodic processes in eustasy, such as tectonism, and in particular the imposition of >10 m amplitude trends at ~1 Myr scales, and much smaller-amplitude changes (<<1 m) at timescales shorter than orbital cycles (Harrison, 2002; Schlager, 2010, see also Miller *et al*., 2005). This is modelled here by imposing long term changes in the orbital sea level signal using realisations of a random walk with a set variance of 9 m, yielding amplitude changes of ~20 m over million year timescales (Fig. 3c). This choice of variance is consistent with the analyses of Miller *et al*. (2005), who determined amplitudes of sea level change of 15-30 m in the Late Cretaceous on million year scales.

EXPERIMENTAL DESIGN

Carbonate accumulation and preservation in the model is controlled by subsidence, erosion, sea level, carbonate production, and lag time. Sea level and carbonate accumulation rate exert the most significant control on available accommodation space in the model, but are poorly constrained in deep time (Bosence and Waltham, 1990; Enos, 1991; Bosscher and Schlager, 1992; Immenhauser, 2005). Erosion and subsidence rates are likely to vary within relatively narrow limits, and vary little over the million-year timescale that the modelling considers. Following Burgess and Pollitt (2012) and Pollitt *et al*. (2014), a parameter space evaluation approach was adopted whereby a range of model scenarios are investigated that encompass a wide gamut of orbital cycle amplitudes and carbonate production rates, thus enabling visualisation of the specific conditions suitable (or otherwise) for preservation of orbital forcing.

To establish the effects of changing sea level amplitude, versions of the insolation-based sea level curve (Fig. 3b) were created with variance ranging from 0.5 to 5.25 m, in 0.25 m increments. These variances yield sea level curves with maximum amplitudes from ~3 m to ~12 m. This range is within the bounds employed by Sømme *et al*. (2009) and Forkner *et al*. (2010) in their modelling of greenhouse carbonate deposition. The ~12 m maximum amplitude is likely at the limit set by non-glacial mechanisms of short-term (<100 ka) eustatic change (Wright, 1992; Miller *et al*., 2005). Quantifying carbonate accumulation rates is hindered by the timespan dependence on carbonate accumulation (Bosscher and Schlager, 1993; Sadler, 1994), owing to incompleteness in the stratigraphic record and potentially also because of environmental factors that limit the sustainability of production (Schlager, 1999). Equally, there are order of magnitude differences in production rates across different parts of a platform (e.g. Bosence and Waltham, 1990). A production rate of ~600 m Myr^{-1} was used as a roughly median production rate in the modelling (following Burgess and Pollitt, 2012 and references therein). As discussed earlier, gross rates of carbonate accumulation in the shallow (<20 m) depths modelled are dominated by euphotic production (Fig. 1). Thus, to assess the influence of differing accumulation rates across a platform or between localities, maximum euphotic production was varied from 240 to 1000 m Myr^{-1} in 40 m Myr^{-1} increments.

With 20 different production rates and 20 different orbital cycle amplitudes, there are 400 model scenarios. Within each scenario, 1000 models were run each with unique realisations of random walk noise and lag times. This number of runs was found to produce statistically stable (i.e. reproducible) results. Throughout the modelling, a model time step of 100 years was used, and models were all 1 Myr long.

DATA ANALYSIS

The key data output in each run of the model are preserved water depths and HFS thicknesses (Fig 3d-f). Preserved water depth data are in the stratigraphic height domain, and sampled at 5 cm sample spacing (Fig. 3d). This sampling interval is comparable to the resolution attained by typical high-resolution cyclostratigraphic studies of outcrop and cored material (e.g. Wu *et al.*, 2013). Following Hill *et al.* (2012), sampled water depth data represent a best-case scenario in which it is assumed that water depth can be inferred exactly from preserved facies. Although impossible to achieve in reality (see in particular recent work by Purkis *et al.*, 2015), this approach isolates only the effects of carbonate production and eustasy on orbital cycle preservation and identification, and does not encompass the errors and information loss that would result from attempting to model the facies response to water depth change.

Multi-taper spectral analysis (using 3 tapers) was used to statistically resolve cyclicities in the sampled water depth data and the HFS thickness data for each model run, (Fig. 3e and f; see Thomson, 1990 and Weedon, 2003 for a summary of the multi-taper method). To report results in the time domain, modelled successions of sampled water depths were fixed to the model duration of 1 Myr by setting the base and top of the succession as 0 and 1 Myr respectively, and resampling at 1 ka intervals (Fig. 3e). This facilitates comparison of model outputs because absolute thicknesses of the generated successions vary, and it places the preserved water depth spectra on the same frequency axis (Fig. 3e). This approach is not the same as tuning individual cycles to fixed (i.e. ~21 ka precession) durations, and the shape of the spectra are the same as would be produced without knowledge of the duration of the succession, (cf. spectra in Fig. 3d and e). The approach is analogous to having an absolute date at the base and top of the modelled succession.

Significance testing of spectral peaks in all the generated spectra was carried out by fitting either a first order autoregressive, AR(1), or white noise function as appropriate to each spectrum, as determined by least squares fitting (e.g. Mann and Lees, 1996; Weedon, 2003; Fig. 3e and f). Peaks in spectra pertaining to high variance at specific frequencies are deemed to reflect significant cycles if they exceed the 95% confidence level set by the expected chi-square distribution of spectral data around the fitted AR(1) or white noise function (Fig. 3e and f). In all the models run here, a conservative approach was adopted that fits an AR(1) or white noise function to the raw spectrum (‘conventional’ AR(1)/white noise modelling, *sensu* Meyers, 2011). Mann and Lees (1996) introduced a modified version of this approach that instead fitted a function to a median smoothed version of the raw spectrum (‘robust’ modelling). The rationale for this was that strong peaks in a spectrum related to cyclicity bias the relative position of the fitted function and the confidence levels. Meyers (2012), however, demonstrated that median smoothing of the raw spectrum could overestimate the significance of peaks at the low end of the spectrum. Exponential HFS thickness distributions were tested for using the Lilliefors test.

RESULTS

Each model run for each model scenario generates a succession of exposure-bound shallow water carbonate HFSs, with these HFSs equating primarily to the precession cycles that dominate the input sea level signal (Figs. 3f and 4). Water depths recorded through each HFS demonstrate that symmetric and asymmetric shallowing upward motifs can occur (Figs. 4 and 5). Maximum modelled water depths range from ~2 m to >7 m (Fig. 6a). Assuming water depths of >1 m are within the subtidal zone (e.g. Burgess *et al*., 2001; Burgess, 2006), the inferred facies developed in the models span intertidal to subtidal environments (Fig. 4). The varying styles of sedimentation and HFS development we have modelled are similar to those explored by Strasser *et al*. (1999) and Hillgärtner and Strasser (2003), who used conceptually similar models of facies development to explain patterns of sedimentation seen in Upper Jurassic to Lower Cretaceous shallow water carbonates in Northern Europe.

Both asymmetric and symmetric HFSs are recognised in real strata, sometimes co-occurring in the same succession (e.g. Balog *et al*., 1997; Hillgärtner and Strasser, 2003). Asymmetric shallowing upward HFSs have been described from Precambrian and Phanerozoic successions (see for example Grotzinger, 1986). In our models, shallowing upward HFSs are well developed when carbonate production rates are high, and accumulation can outpace accommodation space creation (Figs. 4b and d and 5b and d). More symmetric HFSs are associated with low production rates (Figs. 4a and c and 5a and c). Sea level amplitude is a key influence on the relative abundance of subtidal and intertidal facies in a succession (Fig 4). Subtidal dominated HFSs are particularly well developed in model runs that combine low production rates and high sea level amplitudes (Figs. 4c and 5c).

Mean HFS thicknesses across all the model scenarios varies between ~1.7 and ~2.4 m (Fig. 6b), and the mean number of HFSs generated in each model scenario range between 40 and 60 (Fig. 4 and 6c). If each precession cycle in the sea-level signal generated a single HFS there would be 48 HFS preserved in each model (e.g. Fig. 3). The number of HFSs produced in each model run is thus in part a reflection of the overall completeness of the generated succession. Extra HFSs occur when multiple HFSs are generated within a single precession cycle (see discussion section). Relatively few model scenarios generated successions with the same number of HFSs as precession cycles (Fig. 6c), and the conditions best suited to this occupy a narrow band of specific sea level amplitudes and production rates (Fig. 6c).

Orbital cycle preservation

Our approach of analysing 1000 model runs for each model scenario allows the probability of orbital cycle preservation to be calculated for a given scenario to 0.1%. 21 ka precession cycles are well resolved in the preserved water depth data in close to the majority of all model scenarios (Fig. 7a). The example stratigraphies in Figure 4 highlight how precession cycles are particularly well resolved in model scenarios that combine low production rates and high orbital cycle amplitudes (Figs. 4c and 7a). The successions generated under these conditions consist of predominantly subtidal facies, with HFSs generally comprising a subtidal unit capped by a thin intertidal layer followed by an exposure surface. Precession cycles are also typically well resolved in model scenarios that combine low sea level amplitudes and very low production rates (Fig. 7a), with deposition under these conditions dominated by intertidal facies (Fig. 4a). The probability of precession cycle preservation is generally lower under conditions of high production rate (note the often indistinct cycles produced in Fig. 4b and 4d), though never falls below ~25% in any of the model scenarios (Fig. 7a).

Preservation of 100 ka eccentricity cycles follows a similar pattern, but overall the probabilities of eccentricity cycle preservation are lower than for precession (Fig. 7b). Figures 3b and c highlight how eccentricity is not a significant contributor to the variance of insolation forcing, but modulates the amplitude of precession (Fig. 3a). The presence of eccentricity cycles in the preserved water depth data arises from the rectification effect described by Kemp (2011). Figure 3d highlights this effect, and shows how in exposure-prone successions only a fraction of each cycle is preserved (Koerschner and Read, 1989; Sadler, 1994; Kemp, 2011; Eberli, 2013). This imperfect preservation of precession imparts variance at the eccentricity scale in preserved water depths (Fig. 3d). Predictably, in model scenarios with high production rates or low sea level amplitudes, the amplitude of precession is low (i.e. low water depths are maintained, Figs. 4, 5 and 6a), and the rectification effect is also weaker (Fig. 7b).

A further effect of the amplitude modulation of precession and rectification is the preservation of eccentricity-scale cycles in HFS (i.e. precession cycle) thicknesses (Fig. 7c, see also Fig. 3f). These 'bundling' cycles arise because the preserved fraction of each precession cycle that forms an HFS is controlled at least in part by the precession cycle's amplitude (Fig. 3d). Lower amplitude precession cycles tend to produce thinner HFSs (Fig. 3). The analyses indicate that these cycles in HFS thickness are most likely to be preserved in model scenarios that combine high production with high orbital cycle amplitudes (Figs. 7c and 4d). Low rates of production tend to generate HFSs with more consistent thicknesses, and hence weaker bundling cyclicity (e.g. Fig. 4c). The key observation here is that the conditions that best favour the preservation of orbital cycles in preserved water depths and those that favour the preservation of eccentricity-scale HFS thickness bundling are not the same. Fig. 8a shows the probabilities of preserving both eccentricity bundling and precession cycles. These probabilities rarely exceed ~35%, with the highest likelihood associated with high (>4 m) sea level amplitudes and maximum euphotic production rates between ~500 and ~700 m Myr^{-1} (Fig. 8a).

A potentially important control on the observed pattern of orbital cycle preservation is the long-term trends used in the models from the addition of random walk noise. To investigate this, the modelling was repeated without random walk noise in the input sea level signals (Fig. 9). The results of this noise-free modelling indicates a similar pattern of orbital cycle preservation probabilities across the studied parameter space, but with probabilities much higher than in the models with random walk signals added, particularly for the preservation of eccentricity bundling in HFS thickness (cf. Fig. 7 and 9).

The completeness of a succession, as inferred from the number of preserved HFSs (Fig. 6c), has a key impact on the nature of eccentricity bundling (Fig. 8b). Based on the approximate 5:1 frequency ratio between eccentricity (~100 ka) and precession (~21 ka), the expectation is that the number of HFSs per bundle is 5 (Fig. 3a and f), assuming each precession-forced sea level cycle produces a single corresponding HFS. In reality, the mean number of HFSs per bundle varies between ~4.2 and ~5.3 in the parameter space evaluation (Fig. 8b). Indeed, it is apparent from Fig. 7c and Fig. 8b that under conditions where bundles are most likely to be preserved (i.e. high orbital cycle amplitude and high production rates), the expected number of HFSs per bundle would be <5. Similarly, at low sea level amplitudes >48 HFSs per succession is common (Fig. 6c), and the mean number of HFSs per bundle is commonly >5 (Fig. 8b).

Distribution analysis of the HFS thickness data from each model scenario indicates that the majority of model runs in the majority of model scenarios do not produce exponential HFS thickness distributions (Fig. 10a). Rather, analysis of mean *p*-values for each model scenario suggests that indeterminate distributions (i.e. close to exponential) are common (Fig. 10a). There is a clear gradient in the probability of exponential HFS distributions that favours low orbital cycle amplitudes and high production rate conditions, i.e. the opposite of the conditions that favour preservation of orbital cycles in preserved water depth. Exponential HFS thickness distributions and orbital precession cycles in preserved water depths are not mutually exclusive, though coexistence is rare (Fig. 10b). Equally, exponential HFS thickness distributions can also co-exist, albeit very rarely, with bundling cyclicity, particularly at high production rates (Fig. 10c).

DISCUSSION

The model simulates carbonate accumulation governed by processes deemed to be of overarching importance to the preservation of shallow water carbonate strata, i.e. production rate, subsidence, erosion, and sea level. Nevertheless, a range of additional factors that control carbonate accumulation (such as nutrient availability, temperature, and lateral transport) are not explicitly considered. Depth-dependent production profiles are almost certainly more complex than modelled, with a strong species/facies dependence on the true attainable rate of production in a given environment, and marked heterogeneities across the platform (e.g. Bosence and Waltham, 1990; Burgess, 2013; Purkis *et al*., 2015). The model's success in replicating known features of real carbonate successions is the best measure of its efficacy, and within the parameter space evaluation conducted here a wide range of key phenomena are readily simulated, including: 1) metre-scale subtidal to intertidal exposure-capped HFSs, 2) precession and eccentricity driven cycles in water depths/facies, 3) eccentricity-scale HFS thickness bundling, 4) exponential and near-exponential HFS thickness distributions, and 5) combinations of all 4 of these phenomena.

Controls on the preservation of orbital forcing

The results emphasise that the preservation of orbital cycles in peritidal strata is highly sensitive to carbonate production rate and sea level amplitude (Figs. 7 and 9). The probability of orbital cycle preservation generally decreases with lower orbital cycle amplitudes. High production rates further minimise the relative amplitude of preserved water depth cycles by maintaining the platform surface close to sea level (e.g. Fig. 4b). Importantly, the results shown in Figure 9 emphasise how orbital cycle preservation is not guaranteed even under highly idealised conditions without any non-periodic variability in the sea level signal and without long-term trends in accommodation availability (Fig. 9).

In line with the results of Forkner *et al*. (2010) and Kemp (2011), the use of an insolation-based sea level curve enables preservation of eccentricity-scale HFS thickness bundling. Amplitude modulation of precession in the sea level signal is ultimately translated in to the rock record as a frequency modulation of precession (i.e. modulation of HFS thickness), since the amplitude of each precession cycle defines in part the accommodation space available for deposition. Pleistocene records of sea level change highlight how a more complex sea level cycle morphology consisting of large-scale asymmetric ~100 ka cycles with superimposed precession-scale changes can generate similar HFS thickness bundling (Read *et al*., 1986; Goldhammer *et al*., 1987, 1990). In the approach used here, motivated by the likely absence of large-scale asymmetric cycles at ~100 ka scales during greenhouse intervals, similar bundling patterns are as readily produced.

A key finding of the modelling is that the conditions best suited to the preservation of eccentricity-scale HFS thickness bundling are different to the conditions best suited to the preservation of precession and eccentricity cycles in preserved water depth. This result is intuitive, since bundling by definition implies variable preserved precession cycle thicknesses, which has the effect of smearing spectral peaks related to precession and reducing their significance (e.g. Weedon, 2003). The overall probability of preserving eccentricity scale bundling is lower than the probability of preserving water depth cycles. The results of running noise-free versions of the model scenarios (Fig. 9c) demonstrates that this lowered probability is due largely to the effects of long-term trends in the sea level curves, which exert a significant control on preserved HFS thickness. Similarly, randomised lag times, supported by the work of Blanchon and Blakeway (2003), also have an impact on the thickness of HFSs, since the lag time controls in part the fraction of a cycle that is preserved. It is apparent from Figure 7c and Figure 8b that under conditions when bundles are most likely to be preserved (i.e. high sea level amplitude and high production rate), the expected number of HFSs per bundle would be <5, contrary to the 5 HFSs per bundle that the orbital hypothesis predicts. Previous work has noted how bundling patterns in real successions also sometimes deviate from this optimum, with missed cycles the cited cause (e.g. Goldhammer *et al*., 1987, 1990; Osleger and Read, 1991, Vollmer *et al*., 2008). Problematically, however, imperfect and inconsistent bundling patterns may also result from random processes not attributable to an orbital driver (e.g. random long-term sea-level change), suggesting that only when a clear 5:1 bundling is observed in successions can an orbital signal be unambiguously demonstrated. This work, and indeed that of Pollitt *et al*. (2014), emphasises how strict hierarchical patterns and bundling in HFS thicknesses may be rare.

Controls on stratigraphic completeness and implications for astronomical timescale development

Stratigraphic completeness is an important issue in the analysis of peritidal carbonates, since missing cycles ('missed beats') preclude accurate timescale construction, and can have a deleterious affect on the statistical recognition of orbital forcing (e.g. Balog *et al*., 1997). In the modelling, two mechanisms by which precession cycles may be missed can be recognised. In some model runs, notably those with very low production rates, exposure of the platform at precession cycle minima does not occur, or exposure spans a time interval too brief to generate an unambiguous exposure surface (i.e. <1000 years). This results in the representation of two precession cycles as a single HFS. Conversely, cycles may be missed when a platform remains exposed during a precession cycle maxima because the amplitude of that cycle is not sufficient to reflood the platform (Eberli, 2013). A secondary issue demonstrated in the modelling is the development of extra HFSs ('extra beats'). Drummond and Wilkinson (1993b) demonstrated how high rates of production that outstrip the rate of accommodation generation will lead to the platform surface reaching sea level before sea level begins to fall, permitting a further phase of drowning (after a lag period) and development of a second HFS within a single sea level cycle. In the models, the conditions exist for extra HFS to be generated at low sea level amplitudes relative to the amplitude of the imposed random walk variations (Fig. 6c). Figure 6c demonstrates how missed and extra beats are near ubiquitous features of all the models run, and that only a narrow band of conditions exist that are suited to preserving the same number of HFSs as precession cycles. Nevertheless, the preservation of 48 HFSs in the models does not necessarily imply a complete succession, since missed and extra beats can coexist in the same modelled successions.

Taken together, missed and extra beats have a key impact on the utility of shallow water successions for building astronomical timescales. Analysis and tuning of cycles in preserved water depth proxies is a superior way of defining timescales compared to simple HFS counting, since precession cycle boundaries missed due to non-exposure may still be resolvable from high-resolution facies analysis (e.g. Forkner *et al*., 2010), and because recognition of exposure can in any case be complex and equivocal (e.g. Koerschner and Read, 1989; Wilkinson *et al*., 1997b). Conversely, however, the rectification effect that permits preservation of eccentricity cycles in preserved water depth also leads to non-sinusoidal cuspate cycle shapes that generate harmonics at integer multiples of the cycle frequencies (Weedon, 2003; Kemp, 2011; Fig. 3e), potentially leading to a misidentification of orbital parameters or the identification of sub-orbital cycles that are artefacts.

Controls on HFS thickness distributions

The occurrence of exponential HFS and facies thickness distributions in shallow water carbonates has been cited as evidence against orbital forcing acting as the primary driver of metre-scale cycles (Drummond and Wilkinson, 1993a, 1996; Wilkinson *et al*., 1997a, 1997b, 1998). The assumed prevalence of exponential distributions in carbonate strata has been challenged (Burgess, 2008), though distributions at least close to exponential are common (Burgess, 2008). Burgess and Pollitt (2012) and Pollitt *et al*. (2014) have shown that complex facies distributions, including exponential, can arise in purely deterministic models of carbonate accumulation due to the imposition of long term trends and cycles. In the modelling, long-term random walk changes in sea level designed to mimic non-orbital eustatic changes allow the generation of exponential and near exponential HFS thickness distributions (Fig. 10a). The highest probability of preserving such distributions arises at low cycle amplitudes, and hence at a low signal to noise ratio. In models without random walk variations in sea level none of the model runs in any of the model scenarios preserve exponential HFS thickness distributions. The coexistence of unambiguous exponential HFS thickness distributions and orbital forcing can occur, supporting the view of Osleger *et al*. (1994), but this is relatively rare, occurring in only ~5.7% of all model runs (Fig. 10b and c).

CONCLUSIONS

Forward modelling using an insolation-based sea level signal demonstrates how known features of shallow water carbonate successions can be readily simulated, including metre-scale peritidal HFSs, precession and eccentricity driven changes in water depths/facies, and eccentricity-scale HFS thickness bundling. The work emphasises the relative importance of carbonate production rate and sea level amplitude on the preservation of orbital cyclicity. The optimal conditions for the preservation of eccentricity-forced HFS thickness bundling are not the same as the conditions best suited to preservation of orbital cycles in facies/water depths. Moreover, the conditions best suited to preservation of bundling are also associated with stratigraphic incompleteness, leading to the prevalence of bundling motifs with <5 HFSs per bundle. The theoretically perfect preservation of orbital forcing in real successions (i.e. with both eccentricity and precession cycles and eccentricity bundling of five HFSs per bundle) would undoubtedly represent a robust discriminator of orbital influenced sedimentation, but the work indicates that this is unlikely to be a common product of orbital forcing.

The findings are broadly in line with those of Hill *et al*. (2012), and Pollitt *et al*. (2014) who suggest that absent or at least ambiguous evidence for orbital forcing can arise even in successions with strong periodic drivers. Taken together, the results highlight how the sensitivity of orbital preservation to depositional conditions, coupled with the ostensible predisposition of successions to generate complex HFS thickness distributions, may help explain the occurrence of successions in the geological record for which statistical evidence for orbital forcing is ambiguous or absent, even if orbital forcing was a primary driver of accommodation in the depositional environment.

ACKNOWLEDGEMENTS

We are grateful to Andre Strasser, an anonymous reviewer, and Associate Editor Stephen Lokier, who provided helpful comments on an earlier draft of this work.

REFERENCES

Algeo, T. J. and **Wilkinson, B. H.** (1980) Periodicity of mesoscale Phanerozoic sedimentary cycles and the role of Milankovitch orbital modulation, *The Journal of Geology*, **96**, 313-322.

Balog, A., Haas, J., Read, J. F., and **Coruh, C.** (1997) Shallow marine record of orbitally forced cyclicity in a Late Triassic carbonate platform, Hungary, *Journal of Sedimentary Petrology*, **67**, 661–675.

Blanchon, P. and **Blakeway, D.** (2003) Are catch-up reefs an artifact of coring? *Sedimentology*, **50**, 1271-1282.

Bosence, D., Procter, E., Aurell, M., Bel Kahla, A., Boudagher-Fadel, M., Casaglia, F., Cirilli, S., Mehdie, M., Nieto, L., Rey, J., Scherreiks, R., Soussi, M. and **Waltham, D.** (2009) A dominant tectonic signal in high-frequency, peritidal carbonate cycles? A regional analysis of Liassic platforms from Western Tethys. *J. Sed. Res.,* **79**, 389–415.

Bosence, D.W.J. and **Waltham, D.A.** (1990) Computer modeling the internal architecture of carbonate platforms. *Geology*, **18**, 26–30.

Bosscher, H. and Schlager, W. (1992) Computer simulation of reef growth. *Sedimentology*, 39, 503-512.

Bosscher, H. and **Schlager, W.** (1993) Accumulation rates of carbonate platforms. *The Journal of Geology*, **101**, 345-355.

Burgess, P. M. (2001) Modelling carbonate sequence development without relative sea-level oscillations, *Geology*, **29**, 1127-1130.

Burgess, P. M. (2006) The signal and the noise: forward modeling of allocyclic and autocyclic processes influencing peritidal carbonate stacking patterns. *J. Sed. Res.*, **76**, 962–977.

Burgess, P. M. (2008) The nature of shallow-water carbonate lithofacies thickness distributions, *Geology*, **36**, 235–238.

Burgess, P. M. (2013) CarboCAT: A cellular automata model of heterogeneous carbonate strata, *Computers and Geosciences*, **53**, 129-140.

Burgess, P. M. and **Pollitt, D. A.** (2012) The origins of shallow-water carbonate lithofacies thickness distributions: one dimensional forward modelling of relative sea-level and production rate control, *Sedimentology*, **59**, 57-80.

Burgess, P. M., Wright, V. P. and **Emery, D.** (2001) Numerical forward modelling of peritidal carbonate parasequence development: implications for outcrop interpretation, *Basin Res*., **13**, 1-16.

Coe, A. L. (2003) *The sedimentary record of sea-level change*, Cambridge University Press, Cambridge, 288 pp.

Cozzi, A., Hinnov, L.A., and **Hardie, L.A.** (2005) Orbitally forced Lofer cycles in the Dachstein Limestone of the Julian Alps (northeastern Italy), *Geology*, **33**, 789–792.

Drummond, C. N. and **Wilkinson, B.H.** (1993a) Aperiodic accumulation of cyclic peritidal carbonate, *Geology,* **21**, 1023–1026.

Drummond, C.N., and **Wilkinson, B.H.** (1993b) Carbonate cycle stacking patterns and hierarchies of orbitally forced eustatic sea-level change, *Journal of Sedimentary Petrology*, **63**, 369–377.

Drummond, C.N., and **Wilkinson, B.H.** (1996) Stratal thickness frequencies and the prevalence of orderedness in stratigraphic sequences, *Journal of Geology*, **104**, 1–18.

Eberli, G. P. (2013) The uncertainties involved in extracting amplitude and frequency of orbitally driven sea-level fluctuations from shallow water carbonate cycles, *Sedimentology*, **60**, 64-84.

Enos, P., 1991, Sedimentary parameters for computer modeling, in Franseen, E.K., Watney, W.L., and Ross, W., eds., *Sedimentary Modeling: Computer Simulations* *and Methods for Improved Parameter Definition,* State Geological Survey of Kansas, Bulletin **233**, 63–99.

Forkner, R. M., Hinnov, L. A. and **Smart, P.** (2010) Use of insolation as a proxy for high-frequency eustasy in forward modeling of platform carbonate cyclostratigraphy – a promising approach, *Sed. Geol.*, **231**, 1-33.

Gil, J., García-Hidalgo, J. F., Mateos, R. and **Segura, M.** (2009) Orbital cycles in a Late Cretaceous shallow platform (Iberian Ranges, Spain), *Palaeogeography, Palaeoclimatology, Palaeoecology*, **274**, 40-53.

Goldhammer, R.K., Dunn, P.A. and **Hardie, L.A.** (1987) High-frequency glacio-eustatic sea level oscillations with Milankovitch characteristics recorded in Middle Triassic platform carbonates in northern Italy, *Am. J. Sci.*, **287**, 853–892.

Goldhammer, R.K., Dunn, P.A. and **Hardie, L.A.** (1990) Depositional cycles, composite sea-level changes, cycle stacking patterns, and the hierarchy of stratigraphic forcing: examples from Alpine Triassic platform carbonates. *Geol. Soc. Am. Bull.*, **102**, 535–562.

Grotzinger, J.P. (1986) Upward shallowing platform cycles: a response to 2.2 billion years of low-amplitude, high-frequency (Milankovitch band) sea level oscillations, *Paleoceanography*, **1**, 403-416.

Haq, B. U., Hardenbol J. and **Vail, P. R.** (1987) Chronology of fluctuating sea levels since the Triassic, *Science*, **235**, 1156-1167.

Harrison, C. G. A. (2002) Power spectrum of sea level change over fifteen decades of frequency, *Geochem., Geophys., Geosys.*, **3**, DOI:10.1029/2002GC000300.

Hill, J., Wood, R., Curtis, A. and **Tetzlaff, D. M.** (2012) Preservation of forcing signals in shallow water carbonate sediments*, Sed. Geol.*, **275-276**, 79-82.

Hillgärtner, H., and **Strasser, A.** (2003) Quantification of high-frequency sea-level fluctuations in shallow-water carbonates: An example from the Berriasian-Valanginian (French Jura), *Palaeogeography, Palaeoclimatology, Palaeoecology*, **200**, 43–63.

Hinnov, L.A., and **Goldhammer, R.K.** (1991) Spectral analysis of the Middle Triassic Latemar limestone, J. Sed. Petrol*.*, **61***,* 1173-1193.

Immenhasuer, A. (2005) High-rate sea-level change during the Mesozoic: New approaches to an old problem, *Sed. Geol*., **175**, 277-296.

Jacobs, D.K. and **Sahagian, D.L.** (1995) Milankovitch fluctuations in sea level and recent trends in sea-level change: Ice may not always be the answer, in Haq, B., ed., *Sequence stratigraphy and depositional response to eustatic, tectonic and climatic forcing,* Dordrecht, Netherlands, Kluwer, 329–366.

Kemp, D. B. (2011) Shallow water records of astronomical forcing and the eccentricity paradox, *Geology*, 39, 491-494.

Koerschner, W. F. and **Read, J. F.** (1989) Field and modelling studies of Cambrian carbonate cycles, Virginia Appalachians, *J. Sed. Petrol*., **59**, 654-687.

Laskar, J., Robutel, P., Joutel, F., Gastineau, M., Correia, A.C.M. and **Levrard, B.** (2004) A long-term numerical solution for the insolation quantities of the Earth. *Astron. Astrophys*., **428**, 261–285.

Mann, M. E., and **Lees, J. M.** (1996) Robust estimation of background noise and signal detection in climatic time series, *Clim. Change*, **33**, 409-445.

Meyers, S. R. (2012) Seeing red in cyclic stratigraphy: spectral noise estimation for astrochronology, *Palaeoceanography*, DOI:10.1029/2012PA002307.

Miller, K.G., Kominz, M.A., Browning, J.V., Wright, J.D., Mountain, G.S., Katz, M.E., Sugarman, P.J., Cramer, B.S., Christie-Blick, N., and **Pekar, S.F.**

(2005) The Phanerozoic record of global sea-level change, *Science*, **310**, 1293–1298.

Osleger, D. and **Read, J. F.** (1991) Relation of eustasy to stacking patterns of metre-scale carbonate cycles, Late Cambrian, USA, *Journ. Sed. Petrol*., **61**, 1225-1252.

Osleger, D., Drummond, C. N., and **Wilkinson, B. H.** (1994) Aperiodic accumulation of cyclic peritidal carbonate: comment and reply, *Geology*, **22**, 479–480.

Pittet, B. (1994) Mode'le d'estimation de la subsidence et des variations du niveau marin: Un exemple de l'Oxfordien du Jura Suisse, *Eclogae Geol. Helv*., **87**, 513-543.

Pollitt, D.A. (2008) *Outcrop and forward modelling analysis of ice-house cyclicity and reservoir lithologies*. Unpublished PhD Thesis, Cardiff University, Cardiff.

Pollitt, D. A., Burgess, P. M. and **Wright, V. P. (**2014) Investigating the occurrence of hierarchies of cyclicity in platform carbonates, in Smith *et al*., eds., *Strata and time: Probing the gaps in our understanding*. Geological Society, London, Special Publication **404**.

Pomar, L. (2001a) Ecological control of sedimentary accommodation: evolution from a carbonate ramp to rimmed shelf, Upper Miocene, Balearic Islands. *Palaeogeogr. Palaeoclimatol. Palaeoecol*., **175**, 249–272.

Pomar, L. (2001b) Types of carbonate platforms: a genetic approach. *Basin Res*., **13**, 313–334.

Preto, N., Hinnov, L. A., Hardie, L. A., and **De Zanche, V.** (2001) Middle Triassic orbital signature recorded in the shallow-marine Latemar carbonate buildup (Dolomites, Italy), *Geology*, **29**, 1123–1126.

Preto, N., Hinnov, L.A., De Zanche, V., Mietto, P. and **Hardie, L.A.** (2004) The Milankovitch interpretation of the Latemar platform cycles (Dolomites, Italy): Implications for geochronology, biostratigraphy, and Middle Triassic carbonate accumulation, in D'Argenio *et al*., eds., *Cyclostratigraphy: Approaches and case histories*. SEPM Spec. Publ., **81**, 167–182.

Purkis, S.J., Rowlands, G.P. and **Kerr, J.M.** (2015) Unravelling the influence of water depth and wave energy on the facies diversity of shelf carbonates. *Sedimentology*, **62**, 541-565.

Read, J.F., Grotzinger, J.P., Bova, J.A. and **Koerschner, W.F.** (1986) Models for generation of carbonate cycles. *Geology*, **14**, 107–110.

Ruban, D. A. (2014) Mesozoic long-term eustatic cycles and their uncertain hierarchy, *Geosci. Front*., DOI:10.1016/j.gsf.2014.06.001.

Sadler, P. M. (1994) The expected duration of upward-shallowing peritidal carbonate cycles and their terminal hiatuses. *Geological Society of America Bulletin*, **106**, 791-802.

Schlager, W. (1981) The paradox of drowned reefs and carbonate platforms. *Geol. Soc. Am. Bull.*, **92**, 197–211.

Schlager, W. (1999) Scaling of sedimentation rates and drowning of reefs and carbonate platforms, *Geology*, **27**, 183-186.

Schlager, W. (2004) Fractal nature of stratigraphic sequences, *Geology*, **32**, 185-188.

Schlager, W. (2010) Ordered hierarchy versus scale invariance in sequence stratigraphy, *Int. Journ. Earth Sci*., **99**, 139-151.

Schulz, M. and **Schäfer-Neth, C.** (1997) Translating Milankovitch climate forcing into eustatic fluctuations via thermal deep water expansion: a conceptual link, *Terra Nova*, **9**, 228-231.

Sømme, T. O., Helland-Hansen, W. and **Granjeon, D.** (2009) Impact of eustatic amplitude variations on shelf morphology, sediment dispersal, and sequence stratigraphic interpretation: Icehouse versus greenhouse systems, *Geology*, **37**, 587-590.

Strasser, A., **Pittet, B.**, **Hillgartner, H.** and **Pasquier, J-B.** (1999) Depositional sequences in shallow carbonate-dominated sedimentary systems: concepts for a high-resolution analysis, *Sed. Geol*., **128**, 201-221.

Tipper, J. (1997) Modeling carbonate platform sedimentation – lag comes naturally. *Geology*, **25**, 495-498.

Thomson, D. J. (1990) Quadratic-inverse spectrum estimates: applications to paleoclimatology, *Phil. Trans. Roy. Soc. Lond*. A, **332**, 539-597.

Vollmer, T., Ricken, W., Weber, M., Tougiannidis, N., Röhling. H-G. and Hambach, U. (2008) Orbital control on Upper Triassic Playa cycles of the Steinmergel-Keuper (Norian): A new concept for ancient playa cycles, *Palaeogeography, Palaeoclimatology, Palaeoecology*, **267**, 1-16.

Weedon, G. P. (2003) *Time-series analysis and cyclostratigraph,* Cambridge, Cambridge University Press, 259 p.

Wilkinson, B. H., Diedrich, N. W., Drummond, C. N. and **Rothman, E. D.** (1998) Michigan hockey, meteoric precipitation, and rhythmicity of accumulation on peritidal carbonate platforms, *Geol. Soc. Amer. Bull.,* **110**, 1075-1093.

Wilkinson, B. H., Drummond, C. N., Diedrich, N. W. and **Rothman, E. D.** (1997a) Biological mediation of stochastic peritidal carbonate accumulation, *Geology*, **25**, 847-850.

Wilkinson, B. H., Drummond, C. N., Rothman, E. D. and **Diedrich, N. W.** (1997b) Stratal order in peritidal carbonate sequences. *J. Sed. Res*., **67**, 1068–1082.

Wright, V. P. (1992) Speculations on the controls on cyclic peritidal carbonates: ice-house versus greenhouse eustatic controls. *Sedimentary Geology*, **76**, 1-5.

Wu, H., Zhang, S., Hinnov, L. A., Jiang, G., Feng, Q., Li, H. and **Yang, T.** (2013) Time-calibrated Milankovitch cycles for the late Permian, *Nature Communications*, DOI: 10.1038/ncomms3452.

Yang, W. and **Lehrmann, D. J.** (2003) Milankovitch climatic signals in Lower Triassic (Olenekian) peritidal carbonate successions, Nanpanjiang Basin, South China. *Palaeogeography, Palaeoclimatology, Palaeoecology*, **201**, 283-306.

Zühlke, R., Bechstädt, T. and **Mundil, R.** (2003) Sub-Milankovitch and Milankovitch forcing on a model Mesozoic carbonate platform – the Latemar (Middle Triassic, Italy), *Terra Nova*, **15**, 69-80.

Figure captions

Figure 1. Representative **c**arbonate production versus water depth curves for the three carbonate factories modelled. Note how at the low sea level amplitudes explored in the modelling (<20 m), euphotic production dominates, with negligible contribution to total production from oligophotic and aphotic carbonate factories.

Figure 2. Histogram of lag times as output by a single run of the model. The probability distribution of lag times broadly follows that modelled by Blanchon and Blakeway (2003), and reflects a patchy style of platform colonisation. In a single dimension, as modelled in this study, this gives rise to a variable time lag between platform flooding and carbonate accumulation.

Figure 3. Overview of representative signals and spectra used and output by the model. [a] Mean summer insolation at 20°N between 89.94 and 90.94 Ma (Laskar *et*

al., 2004). Note how the spectrum of this signal shows a strong precession component (21 ka period), but no eccentricity (~100 ka) variance. Eccentricity instead modulates the strength of precession. [b] Insolation signal converted to sea level by normalising. [c] Sea level signal with added random walk noise to impose a long-term trend, as well as low variance short-term noise. Magenta line represents the sediment surface as modelled by the model. Note how the spectrum of the sea level signal shows enhanced variance at low frequencies owing to the imposition of this trend, matching closely the spectra of sea level change determined through the work of Harrison (2002) (see main text for details). [d] Modelled preserved water depths versus stratigraphic height as output by the model. Rectification of the sea level signal results in variance at the eccentricity period in the signal (~10 m cycles), as indicated by the power spectrum. [e] Preserved water depths plotted against time. Note how the spectrum is identical to the spectrum of the preserved water depth versus stratigraphic height data (see main text for discussion). Spectrum shows fitted AR(1) model (BG: background) and 95% confidence level (CL). The cuspate (i.e. non-sinusoidal) nature of the analysed signal generates harmonics at integer multiples of the precession frequencies. [f] HFS thicknesses. Each ~2 m precession cycle in [d] preserves a HFS, and the thicknesses of these HFSs show a clear bundling cyclicity, with ~5 cycles per bundle. Spectrum shows how these cycles are statistically significant, as tested against a white noise model.

Figure 4. Example successions generated by the model for four end member modelling scenarios. [a] Example of a succession generated under conditions of low orbital cycle amplitude and low euphotic production rate. Note the clear preservation of ~2 m precession cycles in water depth and how each of these is generally preserved as a single exposure bound HFS. Higher amplitude precession cycles tend to produce

thicker HFSs. [b] Example of a succession generated under conditions of low orbital cycle amplitude and high euphotic production rate. In this scenario, precession cycles are more ambiguous, and water depths remain relatively low. HFS thicknesses are also less consistent, and multiple water depth cycles can be deposited within single HFSs. [c] Example of a succession generated under conditions of high orbital cycle amplitude and low euphotic production rate. In this scenario, precession cycles are extremely well resolved, and tend to produce a single HFS each. HFS thicknesses are also generally consistent. The high sea level amplitude and low production rate results in the deposition of predominantly subtidal facies. [d] Example of a succession generated under conditions of high orbital cycle amplitude and high euphotic production rate. In this scenario, precession cycles are well resolved in preserved water depth but with variable thicknesses, and hence variable HFS thicknesses.

Figure 5. Plot showing the range of morphologies in HFS water depth trends and thicknesses generated from the model under different euphotic production rates and orbital cycle amplitudes. Shallowing upward HFSs dominate at high production rates. High orbital cycle amplitudes generate HFSs with higher water depth amplitudes. The morphologies and thicknesses shown are the average of all HFSs from single model runs.

Figure 6. Parameter space evaluation of key outputs from the model. [a] Mean maximum preserved water depth. Low production rates coupled with high orbital cycle amplitudes preserve the deepest water depths. [b] Mean HFS thicknesses. [c] Mean number of HFS. Note the similarities in the patterns of mean HFS thicknesses and mean number of preserved HFSs. Each cell represents a separate model scenario, and the values plotted are the means of 1000 model runs.

Figure 7. Parameter space evaluation of percentage of model runs that preserve [a] precession cycles in preserved water depth, [b] eccentricity cycles in preserved water depth, and [c] eccentricity-scale cycles in HFS thicknesses (bundles), above the 95% confidence level. Note how the probability of preserving precession cycles is generally higher than the probability of preserving eccentricity cycles, which in turn is higher than the probability of preserving eccentricity bundling in HFS thicknesses. Moreover, note how the conditions best suited to maximising the probability of preserving water depth cycles are different to those best suited to preserving eccentricity bundling (see main text for details). Each cell represents a separate model scenario, and the values plotted are the percentages calculated from 1000 model runs.

Figure 8. [a] Parameter space evaluation of percentage of model runs that preserve both eccentricity HFS thickness cycles (bundles) and precession water depth cycles above the 95% confidence level. Note how the different conditions best suited to preservation of each phenomenon (cf. Fig. 6a and c) leads to a complex grouping of maximum probabilities. [b] Parameter space evaluation of mean number of HFSs per bundle in model runs that preserve evidence for eccentricity bundling cycles above the 95% confidence level. Note how the pattern of mean number of HFSs per bundle across the parameter space is broadly similar to the pattern in mean number of HFSs (Fig. 5c). See main text for details. Each cell represents a separate model scenario, and the values plotted are the percentages or means calculated from 1000 model runs.

Figure 9. Parameter space evaluation of percentage of model runs that preserve [a] precession cycles in preserved water depth, [b] eccentricity cycles in preserved water depth, and [c] eccentricity-scale cycles in HFS thicknesses (bundles), above the 95% confidence level. These results are from model runs without addition of random walk noise. Each cell represents a separate model scenario, and the values plotted are the

percentages calculated from 100 model runs. 100 runs were found to give statistically stable (reproducible) results, in contrast to the 1000 runs needed to evaluate models that had added random walk noise. The only stochasticity in these random walk-free models arises from the random lag times employed. Note that the overall probabilities of preserving orbital forcing in these model scenarios are higher than in the models with added random walk noise, but that the general pattern of probabilities across the analysed parameter space are similar (cf. Fig. 6).

Figure 10. [a] Parameter space evaluation of mean *p*-values associated with the lilliefors test statistic for exponential distribution (distr.) of HFS thicknesses. Conditions best suited to exponential HFS thickness distributions occur at low orbital cycle amplitudes. Indeterminate HFS thickness distributions are prevalent across much of the parameter space. Conditions that provide HFS thickness distributions entirely distinct from exponential occur at low production rates and high orbital cycle amplitudes. [b] Parameter space evaluation of percentage of model runs that preserve both exponential HFS thickness distributions and precession cycles in water depth above the 95% confidence level. [c] Parameter space evaluation of percentage of model runs that preserve both exponential HFS thickness distributions and eccentricity bundling cycles. Note the rarity of model runs that preserve both orbital forcing and exponential HFS thickness distributions. Each cell represents a separate model scenario, and the values plotted are the percentages or means calculated from 1000 model runs.

Kemp et al. (2016) - Figure 1

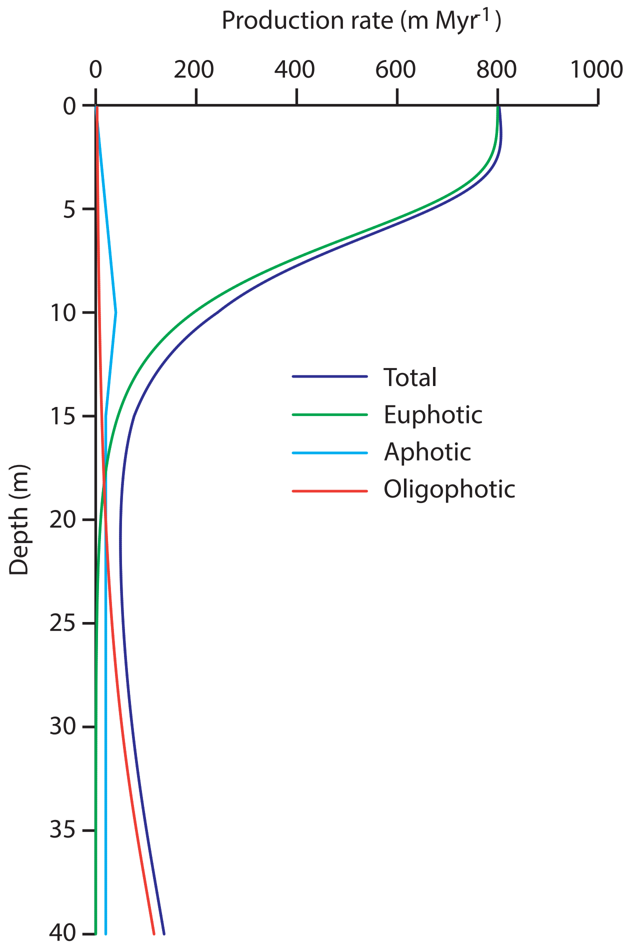

Kemp et al. (2016) - Figure 2

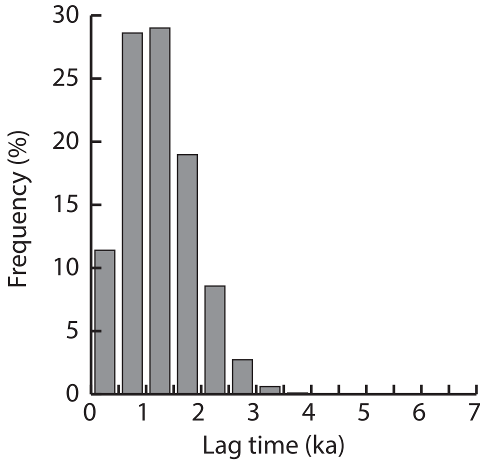

Kemp et al. (2016) - Figure 3

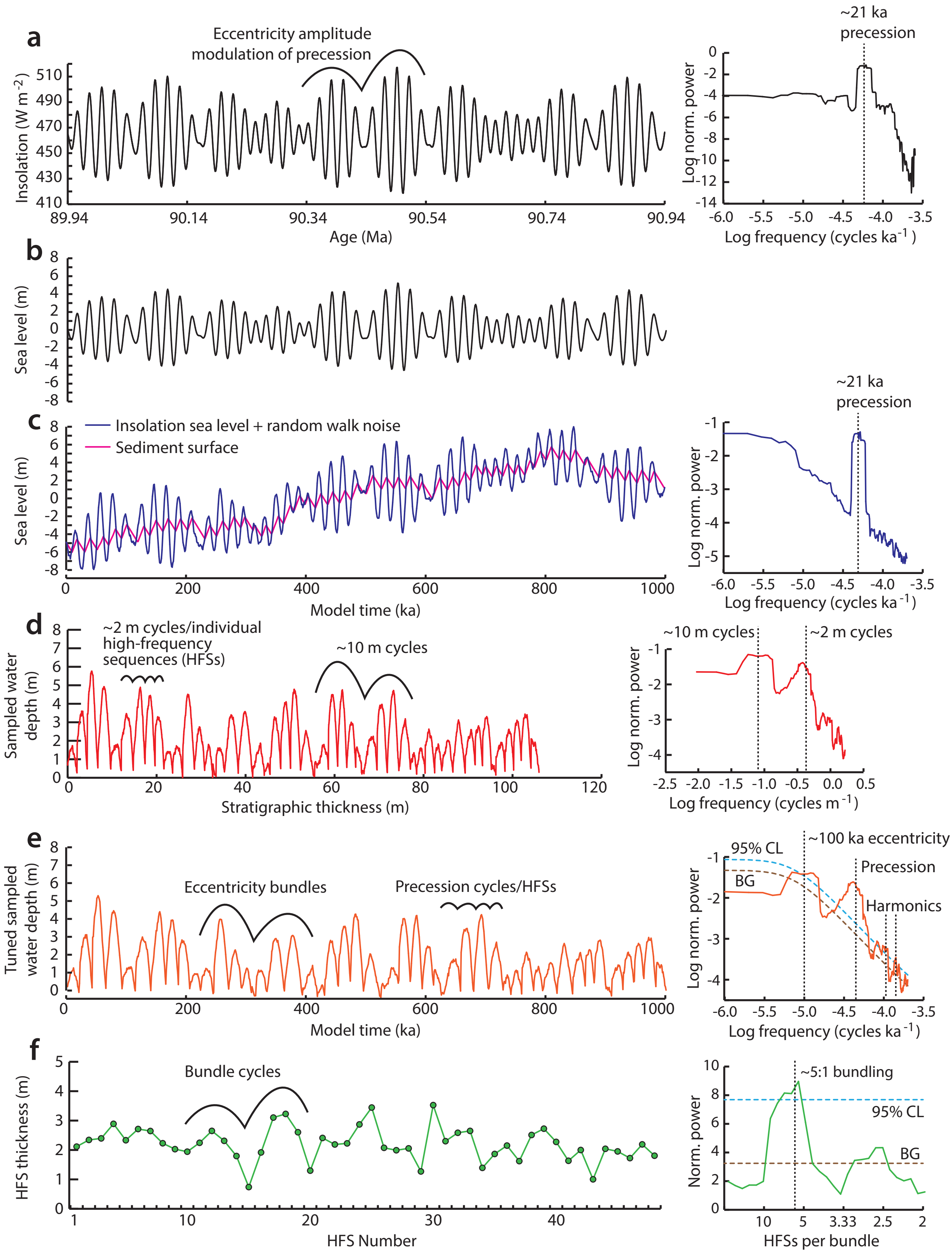

Kemp et al. (2016) - Figure 4

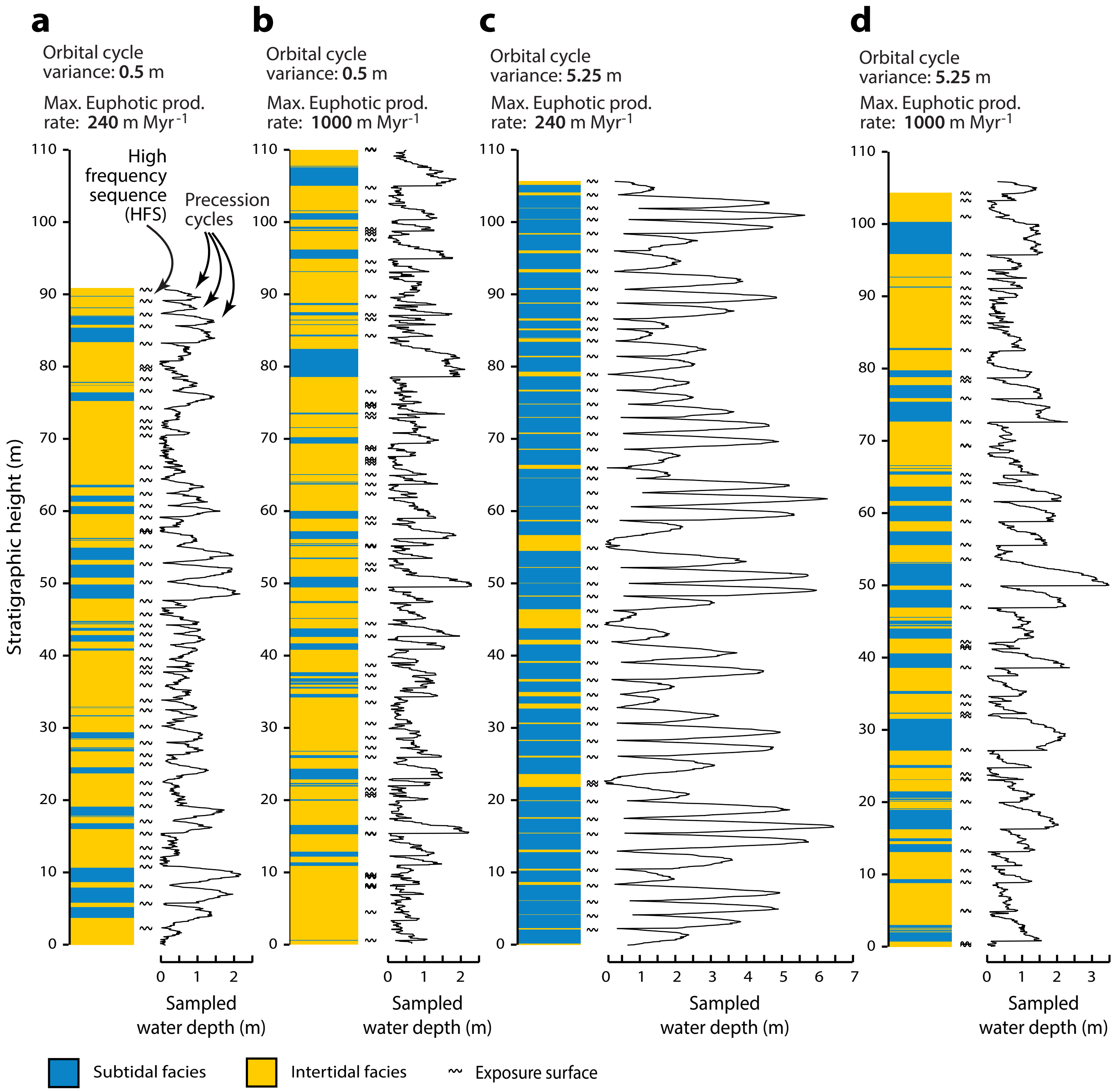

Kemp et al. (2016) - Figure 5

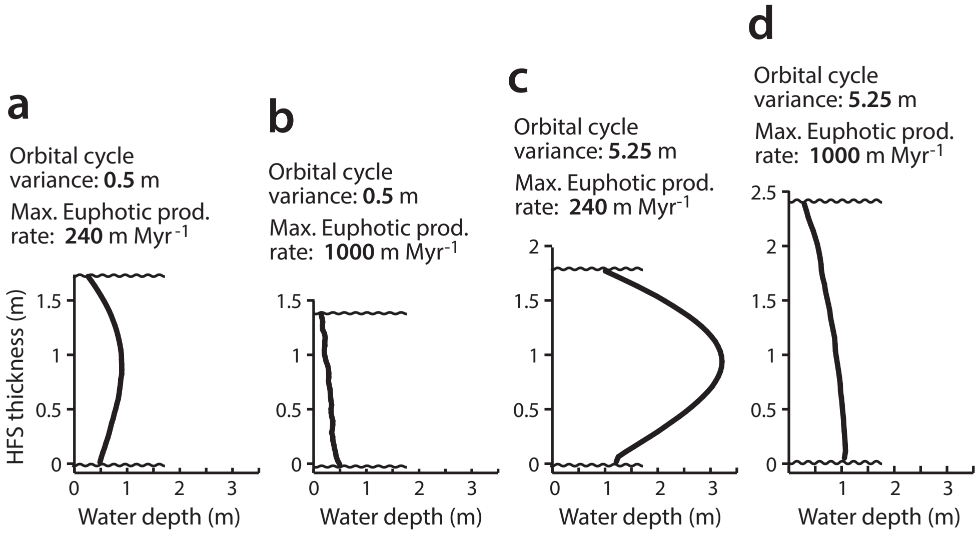

Kemp et al. (2016) - Figure 6

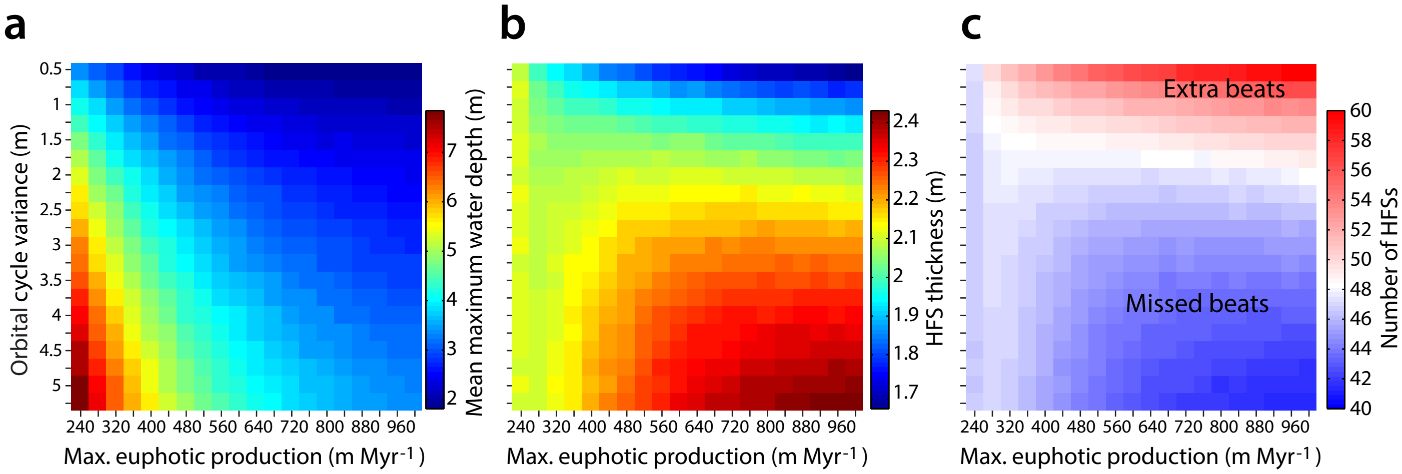

Kemp et al. (2016) - Figure 7

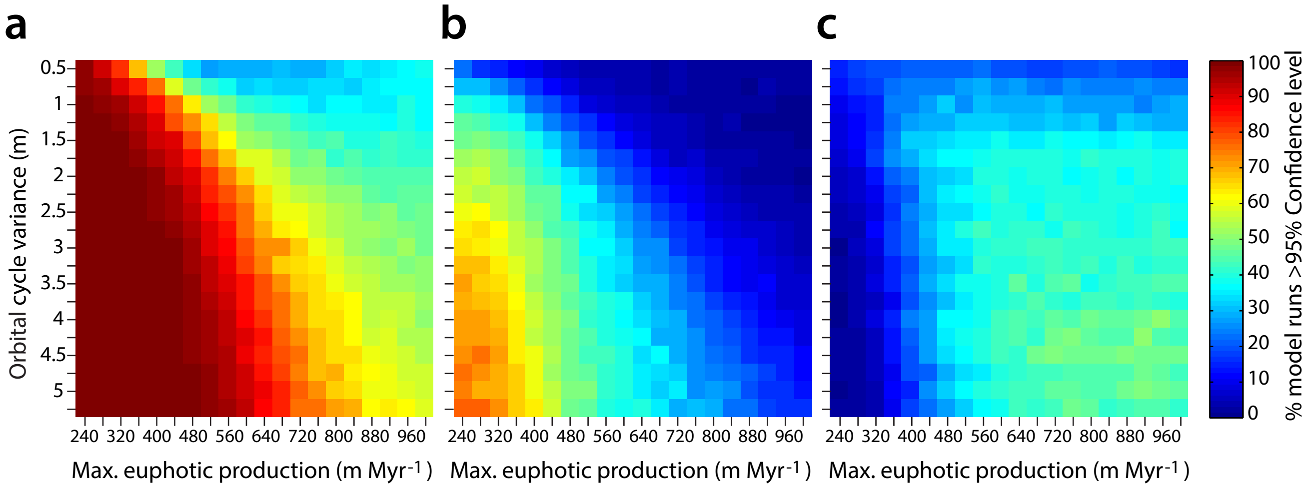

Kemp et al. (2016) - Figure 8

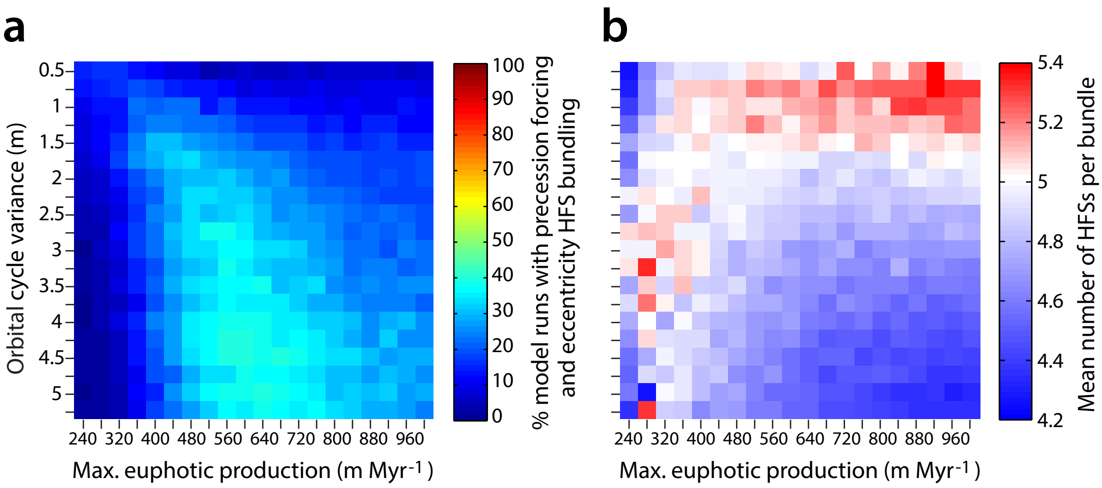

Kemp et al. (2016) - Figure 9

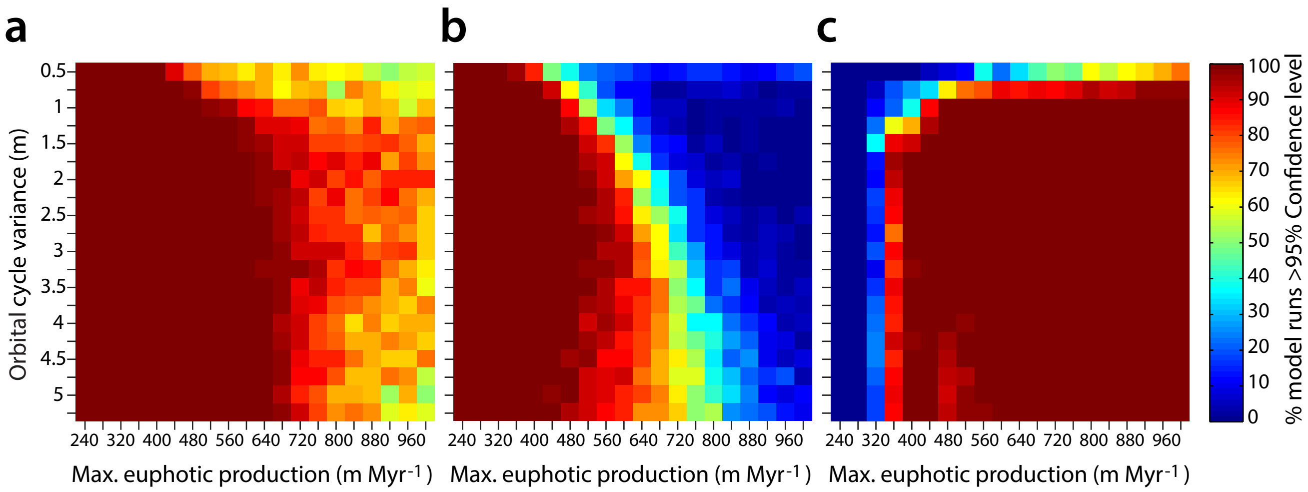

Kemp et al. (2016) - Figure 10